

What flows in the chiral magnetic effect?

— Simulating the particle production with \mathcal{CP} -breaking backgrounds —

Kenji Fukushima

*Department of Physics, The University of Tokyo,
7-3-1 Hongo, Bunkyo-ku, Tokyo 113-0033, Japan*

To address a question of whether the chiral magnetic current is a static polarization or a genuine flow of charged particles, we elucidate the numerical formulation to simulate the net production of right-handed particles and anomalous currents with \mathcal{CP} -breaking background fields which cause an imbalance between particles and anti-particles. For a concrete demonstration we numerically impose pulsed electric and magnetic fields to confirm our answer to the question that the produced net particles flow in the dynamical chiral magnetic effect. The rate for the particle production and the chiral magnetic current generation is quantitatively consistent with the axial anomaly, while they appear with a finite response time. We emphasize the importance to quantify the response time that would suppress observable effects of the anomalous current.

I. INTRODUCTION

In many quantum problems in physics it is highly demanded to establish a numerical framework to simulate full dynamical processes of particle production out of equilibrium. Unsettled and important problems include the leptogenesis and the baryogenesis for the explanation of the baryon asymmetry of the Universe (BAU). It is well-known that Sakharov's three conditions are needed for the BAU; namely, B -breaking process, \mathcal{C} and \mathcal{CP} violation, and out-of-equilibrium. The particle production on top of the electroweak sphaleron [1] accommodates a process with $\Delta(B + L) \neq 0$, which means that $B + L$ decays toward chemical-equilibrium [and this is why the idea based on the SU(5) grand unified theory [2] does not work out for the BAU]. Therefore, if the leptogenesis with some $(B - L)$ -breaking process beyond the Standard Model (see Ref. [3] for example) generates $L \neq 0$ initially, it would amount to $B \neq 0$ finally in chemical-equilibrium. The particle production associated with the sphaleron transition has a character of topological invariance and the index theorem relates the topological number to the change in the particle number. We must recall, however, that the sphaleron is a special static configuration at saddle-point and for more general and non-topological gauge configurations with \mathcal{C} - and \mathcal{CP} -odd components we have to consider microscopic simulations with Weyl fermions. Also, to compute the momentum spectrum of produced particles with arbitrary gauge backgrounds, there is no longer mathematical elegance and some brute-force tactics with numerical simulations is indispensable.

The sphaleron transition rate is proportional to T^4 where T is the temperature [4], and so such topological fluctuations should be abundant also in the strong interaction when the physical system is heated up to $T > \Lambda_{\text{QCD}}$ as argued in Ref. [5]. Such high temperature is indeed realized in the quark-gluon plasma created in the relativistic heavy-ion collision (HIC) experiment. Although the strong interaction does not break \mathcal{CP} (except for negligibly small strong θ), we can still anticipate local violation of \mathcal{P} and \mathcal{CP} before thermal-

ization [6]. This possibility is nowadays referred to commonly as the local parity violation (LPV). Theoretical and experimental challenges are still ongoing about the LPV detection (and no direct evidence has been found for it). Along these lines the recognition of the interplay with pulsed magnetic field \mathbf{B} between two heavy ions was a major breakthrough [7]; \mathbf{B} on top of \mathcal{CP} -odd backgrounds would induce an electric current \mathbf{j} in parallel to \mathbf{B} , which is summarized in a compact formula of the chiral magnetic effect (CME) with chiral chemical potential μ_5 [8]. In a realistic situation of the HIC we can anticipate \mathcal{P} and \mathcal{CP} violation not only from the QCD sphalerons but also from the glasma [9] which is a description of the initial condition of the HIC in terms of coherent fields. Then, without introducing μ_5 that has huge theoretical uncertainty (see Ref.[10] for a recent study with μ_5), we can and should directly compute the anomalous currents associated with the particle production with \mathcal{CP} -odd backgrounds composed from chromoelectric and chromo-magnetic fields [11].

It would be an intriguing attempt to test the CME in a table-top experiment in a way similar to the quantum Hall effect. The biggest difference between the CME and the Hall effect arises from the fact that the carriers of electric charge are not the ordinary particles but chiral particles; that is, a non-zero excess of the right-handed particle number to the left-handed particle number is required [12]. It is quite non-trivial how to implement such a chiral battery (usually represented by $\mu_5 \neq 0$) in materials. Just recently the CME may have been confirmed in a system rather similar to the glasma, in which chirality imbalance is imposed by background fields that break \mathcal{CP} symmetry [13].

Here, to elucidate the motivation of our present study clearly, let us discuss theoretical subtleties about the interpretation of the chiral magnetic (and separation) effect.

1. What carries the electric charge of the current?
In the derivation using the Chern-Simons-Maxwell theory [14] the chiral magnetic current appears in Ampère's law, but it takes a similar form as

Maxwell's displacement current. We know that Maxwell's displacement current is a source for the magnetic field but no charge carrier flows (though the Poynting vector shows a flow of electromagnetic energy) as pointed out in Ref. [15].

2. What is the momentum spectrum of charged particles that flow as the chiral magnetic current? In the derivation using the thermodynamic potential [8] a finite result remains after a cancellation between infinitely large momentum contributions $p^z \sim \pm\infty$, but it is unlikely in any experiment that particles with such large momenta emerge from the vacuum. In the kinetic derivation [16–18] a thermal distribution of particles is finally assumed to retrieve the exact CME coefficient, which provides us with a theoretically correct description of the dynamical current. It is, however, still needed to understand how such a distribution of particles arises. In general with arbitrary (non-thermal) initial conditions the particle distribution functions are not necessarily thermal and then the CME current may not obey the standard formula, which also motivates the numerical simulation.
3. The expression $\langle \Omega | \mathbf{j} | \Omega \rangle \neq 0$ does not always mean a flowing current but it may represent a polarization that is a static expectation value of a vector operator \mathbf{j} , where $|\Omega\rangle$ represents a certain pure state of the physical system. (We can generalize our discussions to mixed states, but the consideration with a pure state suffices for our purpose.) In the lattice-QCD simulation in Euclid spacetime as in Ref. [19], $|\Omega\rangle$ is the Euclidean QCD vacuum, and the current measured with $|\Omega\rangle$ should be a polarization because the current is a non-equilibrium and steady dynamical phenomenon. Actually the chiral separation effect $\langle \Omega | \mathbf{j}_A | \Omega \rangle \propto \mu \mathbf{B}$ has a natural interpretation as a spin polarization [20] (see also Ref. [21] for a recent study on this). To make a possible difference explicit we point out an example found in the computation of the chiral magnetic conductivity $\sigma_\chi(\omega, \mathbf{p})$ that represents a linear response in the presence of spacetime dependent $\mathbf{B}(\omega, \mathbf{p})$. From Fig. 2 of Ref. [22] it is obvious that the static limit $\sigma_\chi(\omega = 0, \mathbf{p} \rightarrow 0)$ takes a value different from the dynamical limit $\sigma_\chi(\omega \rightarrow 0, \mathbf{p} = 0)$.
4. How can the particle motion be aligned to the magnetic field? The conventional explanation (i.e., the correlation between the helicity and the spin alignment under a strong \mathbf{B}) is based on a static picture corresponding to the polarization phenomenon. If there are free right-handed fermions, say, in the direction perpendicular to \mathbf{B} , they just move on a circle with the Larmor radius classically. The spin receives a torque from the Berry's curvature term, but the spin cannot be aligned to \mathbf{B} without dissipation. Also we make a comment that the

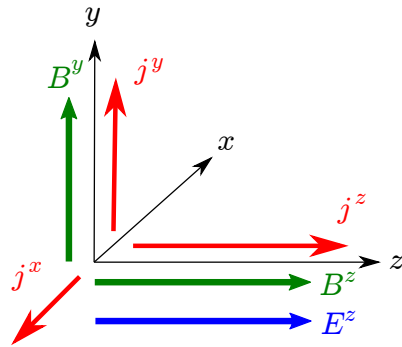


FIG. 1. Schematic view of currents induced by B^y in a \mathcal{CP} -odd domain realized by parallel E^z and B^z . The currents flow in all the x , y , and z directions; j^x is the anomalous Hall current and j^y is the CME current.

kinetic derivation may look like a problem of one-particle motion, but it should be justified by the worldline formalism on the quantum level, and then the (proper) time may be given a meaning different from the genuine time.

5. What is the response time for the chiral magnetic current to get activated? It is unlikely that the current suddenly starts flowing as soon as \mathbf{B} and μ_5 are turned on. (This is actually an unavoidable problem to simulate the chiral magnetic effect assuming a certain μ_5 .) The current generation rate has been calculated only in an idealized setup, and the quantitative estimate of this response time should be crucial for experimental detection in realistic and thus disturbed environments.

To answer these question, in this work, we consider a special setup as illustrated in Fig. 1, which is the schematic view of the CME setup in the HIC and in the condensed matter experiment. The parallel \mathbf{E} and \mathbf{B} (in the z direction in Fig. 1) form \mathcal{P} - and \mathcal{CP} -odd product $\mathbf{E} \cdot \mathbf{B}$, and the CME current j^y is induced in a direction perpendicular to \mathbf{E} , which is reminiscent of the anomalous Hall current j^x . (In this sense one can regard the CME as a 3D extension of the Hall effect.) In the HIC E^z and B^z are Abelian projected chromo-electric and chromo-magnetic fields [11]. In the sphaleron transition these fields are provided from the Abelian projected part of the sphaleron gauge configuration too.

Then, we can address the questions in a very concrete way and we shall present short answers in order:

1. The produced particles from the vacuum fluctuations form a current. The right-handed particles and anti-particles have asymmetric momentum distributions due to $\mathbf{E} \cdot \mathbf{B} \neq 0$, where the particle number is conserved with the opposite excess from the left-handed sector (and the current is doubled). Therefore, the chiral magnetic effect can be realized in a non-equilibrium environment and is most

relevant to the early-time dynamics of the HIC involving the particle production.

2. Produced particles are accelerated by \mathbf{E} and the momentum should have a peak around an impulse given by the product of the Lorentz force times the duration, which is the ordinary situation in the Schwinger mechanism with pure \mathbf{E} . In the same way we can compute the distribution function with $\mathbf{B} \neq 0$ as well as $\mathbf{E} \neq 0$ that is localized in momentum space and so regions with infinitely large momenta are completely irrelevant.
3. The particle production process is the real-time phenomenon out of equilibrium. In this sense, according to our understanding based on the particle production, $\langle \Omega | \mathbf{j}_A | \Omega \rangle \propto \mu \mathbf{B}$ can be interpreted as a dynamical flow of the chirality, which results simply from a different combination of the right-handed and the left-handed sectors of the present calculation. This fact supports the realization of non-zero quadrupole moment of the electric charge suggested from the chiral magnetic wave. We note that if $\langle \Omega | \mathbf{j}_A | \Omega \rangle$ were a spin polarization or a magnetization, there would be no movement of chirality in space, which is not the case in our fully dynamical setup.
4. The particle motion has a peculiar angle distribution or asymmetric momentum distribution (which will be demonstrated in Fig. 2) reflecting the configurations of \mathbf{E} and \mathbf{B} . Thus, unlike the conventional explanation, there is no need to bend the motion of classical particles nor the direction of the spin polarization with \mathbf{B} only.
5. One might think that the asymmetric momentum distribution occurs from the beginning of the particle production and so there is no delay for the topological currents to flow. The plane wave, however, should be deformed into the Landau wave-function after a finite \mathbf{B} is switched on. The response time is governed by the development in the amplitude of the Landau wave-function. In particular the onsets of the particle production and the current generation may look different due to different rates.

II. THEORY OF THE PARTICLE AND CURRENT PRODUCTION

In this work we focus on the right-handed sector only and the current (net particle) density should be doubled (canceled) once the left-handed sector is taken into account. The right-handed Weyl fermion should satisfy the following equation of motion:

$$(i\sigma^\mu \partial_\mu - e\sigma^\mu A_\mu)\phi_R = 0 \quad (1)$$

with $\sigma^\mu = (1, \boldsymbol{\sigma})$. We can readily construct a complete set of plane-wave solutions of Eq. (1) for the asymptotic

states where the interaction is turned off. In general a constant background A_μ may be coupled even without interaction. In the present work we set a gauge that makes $A_0 = 0$ for a technical reason. We can then write positive-energy particle solutions as $\phi_R = u_R(\mathbf{p}; \mathbf{A})e^{-ip \cdot x}$ with

$$u_R(\mathbf{p}; \mathbf{A}) = \begin{pmatrix} \sqrt{|\mathbf{p}_A| + p_A^z} \\ e^{i\theta(\mathbf{p}_A)} \sqrt{|\mathbf{p}_A| - p_A^z} \end{pmatrix} \quad (2)$$

in a certain gauge [or a convention for the overall U(1) phase]. Here we defined $\mathbf{p}_{\pm A} \equiv \mathbf{p} \mp e\mathbf{A}$ and the phase factor is:

$$e^{i\theta(\mathbf{p}_A)} = \frac{p_A^x + ip_A^y}{\sqrt{(p_A^x)^2 + (p_A^y)^2}}. \quad (3)$$

We can identify the anti-particle state from $\phi_{\bar{R}} = -i\sigma^2 \phi_R^*$, which leads to a relation: $u_{\bar{R}}(\mathbf{p}; \mathbf{A}) = u_R(-\mathbf{p}; \mathbf{A})$. In the same way we can find the negative-energy particle and anti-particle solutions with $\phi_{R/\bar{R}} = v_{R/\bar{R}}(\mathbf{p}; \mathbf{A})e^{+ip \cdot x}$, which results in $v_R(\mathbf{p}; \mathbf{A}) = -e^{-i\theta(\mathbf{p}_A)}u_R(\mathbf{p}; -\mathbf{A})$ and $v_{\bar{R}}(\mathbf{p}; \mathbf{A}) = -e^{-i\theta(\mathbf{p}_A)}u_R(-\mathbf{p}; -\mathbf{A})$. We note that $u_R(\mathbf{p}; \mathbf{A})$ and $v_{\bar{R}}(\mathbf{p}; \mathbf{A})$ have an energy $\pm|\mathbf{p}_A|$, while other two, $u_{\bar{R}}(\mathbf{p}; \mathbf{A})$ and $v_R(\mathbf{p}; \mathbf{A})$, have an energy $\pm|\mathbf{p}_{-A}|$.

For the problem of particle and anti-particle production we evaluate an amplitude for the transition from a negative-energy state (with momentum \mathbf{p} and vector potential \mathbf{A}) to a positive-energy state (with momentum \mathbf{q} and vector potential \mathbf{A}'), which we can explicitly express as

$$\begin{aligned} \beta_{\mathbf{q}, \mathbf{p}} &= \int d^3\mathbf{x} \frac{u_R^\dagger(\mathbf{q}_{A'})e^{i|\mathbf{q}_{A'}|x^0 + i\mathbf{q} \cdot \mathbf{x}}}{\sqrt{2|\mathbf{q}_{A'}|}} g_{-\mathbf{p}}(x^0, \mathbf{x}), \\ \bar{\beta}_{\mathbf{q}, \mathbf{p}} &= \int d^3\mathbf{x} \frac{u_{\bar{R}}^\dagger(\mathbf{q}_{-A'})e^{i|\mathbf{q}_{-A'}|x^0 + i\mathbf{q} \cdot \mathbf{x}}}{\sqrt{2|\mathbf{q}_{-A'}|}} \bar{g}_{-\mathbf{p}}(x^0, \mathbf{x}) \end{aligned} \quad (4)$$

for the particles and the anti-particles, respectively. We here introduced new functions, $g_{\mathbf{p}}(x)$ and $\bar{g}_{\mathbf{p}}(x)$, as solutions of the particle and the anti-particle equations of motion satisfying the following negative energy boundary conditions:

$$\begin{aligned} g_{\mathbf{p}}(x) &\longrightarrow \frac{v_R(\mathbf{p}_{-A})e^{i|\mathbf{p}_{-A}|x^0 - i\mathbf{p} \cdot \mathbf{x}}}{\sqrt{2|\mathbf{p}_{-A}|}}, \\ \bar{g}_{\mathbf{p}}(x) &\longrightarrow \frac{v_{\bar{R}}(\mathbf{p}_A)e^{i|\mathbf{p}_A|x^0 - i\mathbf{p} \cdot \mathbf{x}}}{\sqrt{2|\mathbf{p}_A|}} \end{aligned} \quad (5)$$

for x^0 around the initial time in the past. It should be noted that the equation of motion for the anti-particle is not Eq. (1) but e is replaced with $-e$ and σ^μ with $\bar{\sigma}^\mu$. Finally we can express the net particle number (i.e. the particle number minus the anti-particle number *in the right-handed sector*) as well as the spatial currents in the following manner (after dropping the zero-point

oscillation term from J^0 :

$$\begin{aligned} J^0 &= e \int \frac{d^3 \mathbf{q}}{(2\pi)^3} [f(\mathbf{q}) - \bar{f}(\mathbf{q})], \\ \mathbf{J} &= e \int \frac{d^3 \mathbf{q}}{(2\pi)^3} \left[\frac{\mathbf{q}_{A'}}{|\mathbf{q}_{A'}|} f(\mathbf{q}) - \frac{\mathbf{q}_{-A'}}{|\mathbf{q}_{-A'}|} \bar{f}(\mathbf{q}) \right], \end{aligned} \quad (6)$$

where the distribution functions $f(\mathbf{q})$ and $\bar{f}(\mathbf{q})$ above are defined with the amplitudes integrated over all incoming momenta, i.e.,

$$f(\mathbf{q}) \equiv \int \frac{d^3 \mathbf{p}}{(2\pi)^3} |\beta_{\mathbf{q}, \mathbf{p}}|^2, \quad \bar{f}(\mathbf{q}) \equiv \int \frac{d^3 \mathbf{p}}{(2\pi)^3} |\bar{\beta}_{\mathbf{q}, \mathbf{p}}|^2. \quad (7)$$

These functions are naturally given an interpretation as the distribution functions of particles and anti-particles. We note that J^0 above is a formula equivalent to that as utilized in Ref. [23]. We also make a comment on the relation to the chiral kinetic theory where the current is defined with $\dot{\mathbf{x}}$ and the equation of motion solves $\dot{\mathbf{b}}\mathbf{x}$ in terms of \mathbf{q} and an additional contribution from Berry's curvature. The appearance of the *canonical* momenta $\mathbf{q}_{A'}$ (shifted by \mathbf{A}') in Eq. (6) corresponds to using $\dot{\mathbf{b}}\mathbf{x}$ on the level of the equation of motion. Still, it is highly non-trivial how to see the analytical relation between two approaches, which will be an interesting future problem.

III. SIMULATION SETUP

We here consider pulsed fields approximated by step functions for a duration T . We choose the origin of the time so that we start solving Eq. (1) numerically from $t = 0$. Introducing a temporal profile defined by

$$\epsilon(t) \equiv \begin{cases} 1 & (-T/2 \leq t - t_0 \leq T/2) \\ 0 & (|t - t_0| > T/2), \end{cases} \quad (8)$$

we can explicitly specify the electric and magnetic fields that we want to consider here as

$$E^z(t) \sim B^z(t) \sim B^y(t) \propto \epsilon(t). \quad (9)$$

This choice of the temporal profile is motivated based on the glasma dynamics in which both the external magnetic field and the chromo-fields decay within the same time scale of $\sim 0.1 \text{ fm}/c$ [24, 25]. Theoretically speaking, to define the produced particle number uniquely, we should setup the asymptotic states where interaction is switched off. We also mention another possibility to prescribe the particle number in a transient state (mostly relying on an adiabatic approximation) as studied in Ref. [26], though we do not adopt it.

It is, however, technically non-trivial how to realize the external fields as Eq. (9) strictly. Here, we will make a simpler choice of the gauge potentials:

$$\begin{aligned} A^x &= B_\perp \epsilon(t) z - B_\parallel \epsilon(t) y, \quad A^y = 0, \\ A^z &= -E_0 \bar{\epsilon}(t), \end{aligned} \quad (10)$$

where $\bar{\epsilon}(t) = \int_{-\infty}^t \epsilon(t') dt'$. We note that $A^z(t = -\infty) = 0$ and $A^z(t = \infty) = -E_0 T \neq 0$ and this is why we should keep \mathbf{p}_A in all the expressions for produced particles. The above vector potentials actually lead to the magnetic fields as almost desired:

$$B^x(t) = 0, \quad B^y(t) = B_\perp \epsilon(t), \quad B^z(t) = B_\parallel \epsilon(t), \quad (11)$$

whereas the electric fields have some extra components:

$$\begin{aligned} E^x(t) &= -B_\perp \epsilon'(t) z + B_\parallel \epsilon'(t) y, \quad E^y(t) = 0, \\ E^z(t) &= E_0 \epsilon(t). \end{aligned} \quad (12)$$

We chose the gauge (10) so that we can have $E^y(t) = 0$ because we are interested in j^y . This also indicates that the current j^x has not only the anomalous component but a finite contribution induced by $E^x \neq 0$.

We note that in our present calculation we neglect the back-reaction and so this j^x would not affect j^y . Because we start the simulation with the null initial condition with zero particle, this approximation for the back-reaction is expected to hold well especially for our setup with pulsed fields. In principle our formulation can be upgraded to the classical statistical simulation containing back-reaction [27] or the Dirac equations can be combined with a numerical solution of Maxwell's equations. The classical evolution suffices for our present purpose to figure out the net particle production and associated CME current generation.

Let us now go into some more technical parts. It is convenient to keep the reflection symmetry of axes in order to avoid non-vanishing currents due to lattice artifact. A perturbation theory in terms of A^i would give a term like $\propto z, y$ that should be vanishing after the spatial integrations. This can be non-perturbatively realized on the lattice by the periodicity of the link variables. Alternatively, if we take the spatial sites n^i (that gives $x^i = n^i a$ with the lattice spacing a) from $-N_i$ to $+N_i$ for $i = x, y, z$, these terms $\propto z, y$ trivially disappear. The spatial volume is thus $(2N_x + 1) \cdot (2N_y + 1) \cdot (2N_z + 1) \cdot a^3$ in the present simulation. The corresponding momenta are discretized as $p^i a = 2\pi k^i / (2N_i + 1)$. We also note that we impose the anti-periodic boundary condition to avoid the singularity at $|\mathbf{p}_A| = 0$ in Eq. (2) or in Eq. (3). This means that k^i should take half integral values from $-N_i + 1/2$ to $+N_i + 1/2$. We emphasize here that, if the spatial volume is large enough, it does not matter whether the boundary condition is periodic or anti-periodic. This is simply a prescription not to hit the singularity at $|\mathbf{p}_A| = 0$. One might think that one could insert a small regulator in the denominator like the $i\epsilon$ prescription. Indeed, one could adopt the periodic boundary condition and could take an average of contributions from six neighbors, $p_A^x = \pm\epsilon$, $p_A^y = \pm\epsilon$, $p_A^z = \pm\epsilon$ around $|\mathbf{p}_A| = 0$. As seen in momentum space, however, such an averaging procedure is effectively identical to imposing the anti-periodic boundary condition. In any case we should carefully treat the singularity at $|\mathbf{p}_A| = 0$ because this infrared singularity

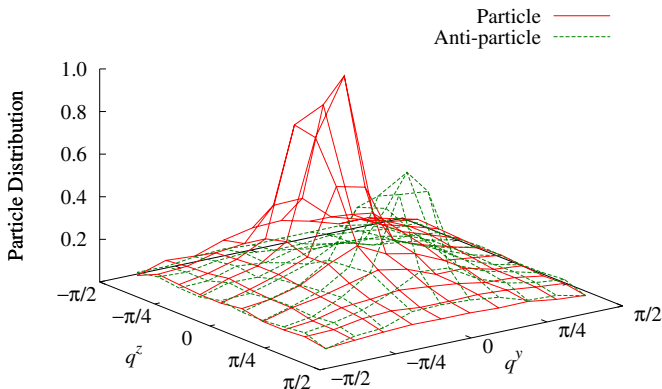


FIG. 2. Distribution of the produced particles and anti-particles as functions of q^y and q^z (and integrated with respect to q^x ; see the text). The lattice size is $N_x = N_y = N_z = 12$ and the magnetic fields are $B_{\parallel} = B_{\perp} = E_0/2$.

is responsible for the axial anomaly, which is manifested in the representation with Berry's curvature [16–18].

If we integrate over all momenta, we cannot avoid picking up all contributions from the doublers and the net particle production should be then absolutely zero because the axial anomaly is exactly canceled according to the Nielsen-Ninomiya theorem [28]. It is thus crucial to get rid of the doubler contributions properly. To this end we limit our momentum integration range to the half Brillouin zone only, i.e., k^i from $-N_i/2 + 1/2$ to $+N_i/2 - 1/2$ (which is used in Ref. [23] too). We note that the axial anomaly is correctly captured from the singular contributions in the wave-function around $|\mathbf{p}_A| = 0$, though it usually appears near the ultraviolet cutoff in a diagrammatic approach. (We have numerically checked that our results are robust against small shifts at the momentum edges, which is also understandable from Fig. 2; produced particles are centered with small momenta.) One should not be confused with the situation in Euclidean, i.e., static lattice simulation in which the whole Dirac determinant should be evaluated to identify the statistical weight for gauge configurations. For the present purpose, in contrast, we need the information on each momentum mode, and so the computation is much more time consuming than evaluating the determinant, but it is easier to get rid of the doublers on the mode-by-mode basis.

When we change the lattice size and the lattice spacing a , we should change a dimensionless $E_0 a^2$ accordingly to fix E_0 in the physical unit. In this work we choose a reference lattice size as $N_x = N_y = N_z = 8$ (i.e., 17^3 lattice volume) and scale physical quantities such as $E_0 a^2 \propto 17^2/(2N+1)^2$ with varying $N_x = N_y = N_z = N$. To simplify the notation let us absorb e in the field definition and omit a hereafter. Then, we take $E_0(N=8) = 0.1$ and change B_{\parallel} and B_{\perp} from 0 to E_0 . We set the duration as $T = \sqrt{10/E_0}$ (that is, $T = 10$ for $N = 8$). Our choice of t_0 is $t_0 = 0.6T$ and we continue solving Eq. (1) up to $t = 1.2T$ with time spacing $\Delta t = 0.02T$ using the

2nd-order Runge-Kutta method (with which we carefully checked that the accuracy is good enough for our present simulation).

We did not quantize the field strength unlike Ref. [29]. Actually we compared results with unquantized and quantized fields (in the unit of $2\pi/N_x N_y$ for B_z etc) and found that this would make only negligible difference. Because our calculation is classical for gauge fields, non-quantization of the field strength is harmless for our numerical results, and moreover, technically speaking, we do not have to impose a boundary condition for the gauge fields unless we solve the equation of motion containing the derivatives of the gauge fields.

Even if $B_{\parallel} = B_{\perp} = 0$, a finite E_0 would induce the pair production of particles and anti-particles under the Schwinger mechanism (see Ref. [30] for a comprehensive review). Because we deal with Weyl fermion, the pair production is always possible for any $E_0 \neq 0$, which leads to a finite distribution of particles with $-E_0 T \lesssim p^z \lesssim 0$ and $p^x = p^y = 0$ (and with $0 \lesssim p^z \lesssim E_0 T$ for anti-particles). If B_{\parallel} or B_{\perp} is finite, this distribution is smeared in momentum space as clearly observed in Fig. 2 in which we present $\int (dq^x/2\pi) f(\mathbf{q})$ and $\int (dq^x/2\pi) f(\mathbf{q})$ as functions of q^y and q^z in the case with $B_{\parallel} = B_{\perp} = E_0/2$. In addition to smearing, it is evident in Fig. 2 that the particle is more enhanced over the anti-particle because of the \mathcal{CP} -odd background, which signals for the net production of right-handed particles. (For the vector gauge theory the total particle number is conserved as a result of summing right-handed and left-handed contributions up.)

To close this section we shall make some remarks about the lattice convention. Taking the sum over dimensionless momenta k^i corresponds to the phase-space integral $V \int d^3\mathbf{p}/(2\pi)^3$. In our definition $\beta_{\mathbf{q},\mathbf{p}}$ has a mass dimension of V and so $f(\mathbf{p})$ has a mass dimension of V too. Then, J^0 and \mathbf{J} become dimensionless quantities. In these final expressions, however, the prescription to avoid the doubler contributions makes the phase-space volume smaller by a factor $N^3/(2N+1)^3$, which should be corrected in the end. In this paper we would not show the lattice version of expressions, but for example, $q_{\pm A}^i$ in Eq. (6) should be understood as $\sin[(q^i \mp A^i)a]$.

IV. NUMERICAL RESULTS

In what follows we normalize $j^0 = J^0/V$ and $\mathbf{j} = \mathbf{J}/V$ by the following quantity:

$$n_0 = \frac{E_0^2}{4\pi^3} \cdot T, \quad (13)$$

which is the pair production rate $E_0^2/4\pi^3$ in the Schwinger mechanism multiplied by the duration T , which gives us a natural order-of-magnitude estimate. Then, j^0/n_0 should remain to be a reasonable number, which is confirmed in Fig. 3.

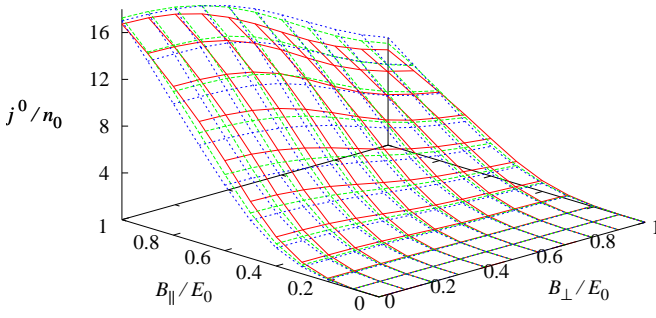


FIG. 3. Net particle density j^0 normalized by n_0 in Eq. (13) as a function of B_{\parallel} and B_{\perp} . The lattice size is $N_x = N_y = N_z = 8, 10, 12$ from the bottom (solid) to the top (dotted).

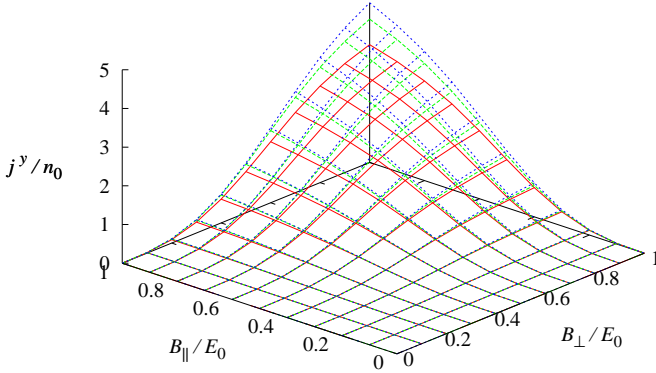


FIG. 4. Net current density j^y normalized by n_0 which is to be interpreted as the CME current.

Figure 3 clearly evidences for a non-zero value of the net particle production for $\mathbf{E} \cdot \mathbf{B} = E_0 B_{\parallel} \neq 0$. We can make it sure that the net particle production is vanishing when $B_{\parallel} = 0$. This should be trivially so but a non-symmetric treatment of coordinates would pick up unphysical artifact, which is not the case in the present simulation. In Fig. 3 the lattice size is $N_x = N_y = N_z = 8, 10, 12$ (i.e., $17^3, 21^3, 25^3$ lattice volumes) from the bottom (solid) to the top (dotted). We can conclude that N_i dependence is rather mild, while it is still there. In fact j^0 shows moderate dependence on B_{\perp} , which results from the lattice artifact. In the steady system with constant electromagnetic fields the anomalous particle production rate has only weak dependence on B_{\perp} and it slightly increases with increasing B_{\perp} . We can see a tendency that j^0 at smaller (larger) B_{\perp} is pushed down (up) as N_i increases.

Now we are going to discuss \mathbf{j}/n_0 obtained in our numerical calculation. Here let us focus only on the chiral magnetic current j^y and postpone discussions about the anomalous Hall current j^x and Ohm's current j^z to a separate publication [31]. It is interesting that our results in Fig. 4 surely represents a non-zero CME current as theoretically expected. We see that $j^y = 0$ when either B_{\parallel} or B_{\perp} is vanishing. Because j^y is the CME current, it is naturally vanishing if $B_{\perp} = 0$. Furthermore, $B_{\parallel} = 0$

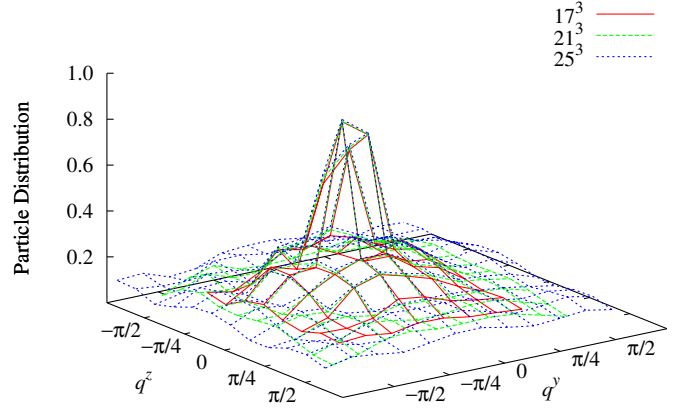


FIG. 5. Distribution of the produced particles as functions of q^y and q^z (and integrated with respect to q^x) for different lattice sizes $17^3, 21^3$, and 25^3 . The magnetic fields are $B_{\parallel} = B_{\perp} = E_0/2$ and the duration is $0.5T$.

means $\mathbf{E} \cdot \mathbf{B} = 0$, and so, no *net* particle production is allowed (even though the *pair* production is possible as long as $\mathbf{E} \neq 0$). The current is vanishing then due to the lack of electric carrier.

V. LATTICE-SIZE DEPENDENCE AND THE RESPONSE TIME

The lattice-size dependence that we have seen is the ultraviolet extrapolation, for which the box size is fixed and the lattice spacing is decreased. Therefore, E_0 in the unit of the lattice spacing was rescaled to fix the observables in the physical unit. In the present case the numerical results should be stable for the ultraviolet extrapolation. We can understand this from Fig. 5. As mentioned before, the distribution function is well localized in momentum space, and so the contributions from the high-momentum region simply attach a tail in the particle distribution as shown in Fig. 5.

In our definition $f(\mathbf{q})$ does not go to zero for $|\mathbf{q}| \rightarrow \infty$ when $\mathbf{E} \neq 0$ and $\mathbf{B} \neq 0$. If the subtraction of the zero-point oscillation energy is normalized at $|\mathbf{q}| \rightarrow \infty$ we could remove an irrelevant shift in the distribution function. In principle, however, such a constant shift does not affect j^0 and \mathbf{j} : the particle and the anti-particle contributions cancel for J^0 and there is no contribution to the angle integration of $\int d^3\mathbf{p}$ for \mathbf{j} . From this consideration we can expect better ultraviolet convergence for \mathbf{j} because a constant shift vanishes for each of the particle the anti-particle parts, while j^0 needs a delicate cancellation. We will see that this expectation is indeed the case in our numerical simulation.

It would be of pragmatic importance to consider j^0 and j^y as a function of the pulse duration, that is, the life time of the external fields. So far, we fixed it as $T = \sqrt{10}/E_0$ and let us vary it now. Theoretically speaking, for a sufficiently large duration, we should expect linear de-

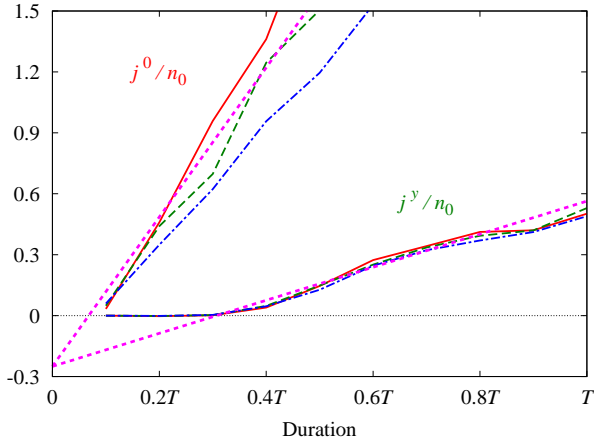


FIG. 6. Profile of j^0 and j^y as a function of the pulse duration normalized by n_0 . The lattice size is $N = 8$ (solid line), 10 (dashed line), 12 (dash-dotted line). The magnetic fields are chosen as $B_{\parallel} = B_{\perp} = E_0/2$. The dotted line represents the analytically estimated rates for the particle production and the current generation (with a common offset -0.25).

pendence assuming constant rates of particle production and current generation. In contrast, for a small duration, it is very difficult to predict what should happen *a priori*, and this is why we must perform the numerical simulations.

Our numerical results in Fig. 6 (for $N = 8, 10, 12$ corresponding to $17^3, 21^3, 25^3$) where $B_{\parallel} = B_{\perp} = E_0/2$ is fixed clearly confirm linear dependence for large duration (apart from small oscillation which is characteristic to magnetic phenomena). Although j^0 shows some lattice-size dependence (due to the constant shift in the ultraviolet region of the produced particle distribution), two results for j^y with different N_i 's are nearly overlaid to each other. This clearly indicates that, because the constant shift drops off in $\int d^3\mathbf{q}$, j^y has no contamination from the ultraviolet fluctuations.

We find for small duration a region of delay in which j^0 and j^y remain almost vanishing. The presence of such delay is intuitively understandable: it should take some time for the wave-function to transform from the free plane wave to the Landau-quantized one after a sudden switch-on of the magnetic field. We would emphasize that what seems non-trivial in Fig. 6 is that the delay for j^y is more than three times larger than that for j^0 . In our interpretation this difference in the onsets comes from the difference in the rates. In Fig. 6 we showed the analytically estimated rates (by the dotted line) using the formula in Ref. [11] with a common offset -0.25 . The onset for j^y is more delayed than that for j^0 since its rate $\partial_t j^y$ is smaller.

Finally we briefly comment on the sensitivity when we change the box size, i.e., the infrared extrapolation. We kept the lattice spacing (and so $E_0 a^2$) and changed the lattice size to find that there is a subtle feature in the

scaling behavior. Since we need to go far into technical details to address this problem, we will leave it for another publication that will be focused on the lattice formulation and the systematic checks of the lattice-size dependence.

VI. SUMMARY AND OUTLOOK

We formulated the production of particles and anti-particles and checked its validity by looking for a right-handed particle excess on \mathcal{CP} -odd backgrounds. We limited our main concern to the CME current at present, but this type of the calculation should be applicable for a wider range of physical problems. For example, the (pair) particle creation at the horizon of the acoustic blackhole (see Ref. [32] for a pedagogical article) attracts attention, and it would be feasible to combine it with \mathcal{CP} -odd (or \mathcal{T} irreversible) background effects, for which we can apply our method. Of course, as mentioned in the beginning, possible applications should cover problems of sphaleron-like transitional processes in the electroweak and the strong interactions on top of arbitrary gauge fields including non-topological ones.

Here we emphasize the impact of the agreement between our numerical results and the analytical expressions. It is very non-trivial that a direct evaluation of the current according to Eq. (6) could be consistent with the quantum anomaly. Also we emphasize the importance of real-time character of the chiral magnetic current generation. The physical interpretation and the theoretical estimate of μ_5 are quite problematic and sometimes misleading in the literature. Our successful simulation is the first step toward a realistic simulation in experimental setups without μ_5 in the system.

In this kind of approach to solve the equation of motion, the anomaly arises from the infrared singularity around $|\mathbf{p}_A| = 0$. The major part of the discretization error might be attributed to underestimating the singular contributions with coarse mesh. This implies that there may be a hybrid way to extract the singular terms analytically and to calculate non-singular parts numerically [31]. This would reduce the lattice-size dependence and we can make theoretical estimates with improved reliability. Though we have confirmed that our CME current is close to the one in the continuum limit, it would be worth developing such a hybrid algorithm. Another direction for the improvement is to include back-reaction from gauge fluctuations. Once the back-reaction is taken into consideration, it would capture the effect of the chiral plasma instability [33]. These are works under progress [31].

ACKNOWLEDGMENTS

This work was partially supported by JSPS KAKENHI Grant Number 15H03652 and 15K13479.

-
- [1] F. R. Klinkhamer and N. S. Manton, Phys. Rev. D **30**, 2212 (1984).
 - [2] M. Yoshimura, Phys. Rev. Lett. **41**, 281 (1978) [Erratum-ibid. **42**, 746 (1979)].
 - [3] M. Fukugita and T. Yanagida, Phys. Lett. B **174**, 45 (1986).
 - [4] P. B. Arnold and L. D. McLerran, Phys. Rev. D **37**, 1020 (1988).
 - [5] L. D. McLerran, E. Mottola and M. E. Shaposhnikov, Phys. Rev. D **43**, 2027 (1991).
 - [6] D. Kharzeev, R. D. Pisarski and M. H. G. Tytgat, Phys. Rev. Lett. **81**, 512 (1998).
 - [7] D. E. Kharzeev, L. D. McLerran and H. J. Warringa, Nucl. Phys. A **803**, 227 (2008).
 - [8] K. Fukushima, D. E. Kharzeev and H. J. Warringa, Phys. Rev. D **78**, 074033 (2008).
 - [9] D. Kharzeev, A. Krasnitz and R. Venugopalan, Phys. Lett. B **545**, 298 (2002).
 - [10] Y. Hirono, T. Hirano and D. E. Kharzeev, arXiv:1412.0311 [hep-ph].
 - [11] K. Fukushima, D. E. Kharzeev and H. J. Warringa, Phys. Rev. Lett. **104**, 212001 (2010).
 - [12] D. Kharzeev and H.-U. Yee, Phys. Rev. **B88**, 115119 (2013).
 - [13] Q. Li, D. Kharzeev, C. Zhang *et al.*, arXiv:1412.6543 [cond-mat.str-el].
 - [14] D. E. Kharzeev, Annals Phys. **325**, 205 (2010).
 - [15] K. Fukushima, Lect. Notes Phys. **871**, 241 (2013).
 - [16] D. T. Son and N. Yamamoto, Phys. Rev. Lett. **109**, 181602 (2012); Phys. Rev. D **87**, no. 8, 085016 (2013).
 - [17] M. A. Stephanov and Y. Yin, Phys. Rev. Lett. **109**, 162001 (2012).
 - [18] J. H. Gao, Z. T. Liang, S. Pu, Q. Wang and X. N. Wang, Phys. Rev. Lett. **109**, 232301 (2012); J. W. Chen, S. Pu, Q. Wang and X. N. Wang, Phys. Rev. Lett. **110**, no. 26, 262301 (2013).
 - [19] A. Yamamoto, Phys. Rev. Lett. **107**, 031601 (2011).
 - [20] In private communications with Igor Shovkovy and Naoki Yamamoto.
 - [21] N. Yamamoto, arXiv:1502.01547 [cond-mat.mes-hall].
 - [22] D. Kharzeev and H.J. Warringa, Phys. Rev. D **80**, 034028 (2009).
 - [23] F. Gelis, K. Kajantie and T. Lappi, Phys. Rev. C **71**, 024904 (2005); Phys. Rev. Lett. **96**, 032304 (2006).
 - [24] T. Lappi and L. McLerran, Nucl. Phys. A **772**, 200 (2006).
 - [25] K. Fukushima, Phys. Rev. C **76**, 021902 (2007) [Phys. Rev. C **77**, 029901 (2007)].
 - [26] N. Tanji, Annals Phys. **324**, 1691 (2009); Annals Phys. **325**, 2018 (2010).
 - [27] F. Hebenstreit, J. Berges and D. Gelfand, Phys. Rev. Lett. **111**, 201601 (2013); V. Kasper, F. Hebenstreit and J. Berges, Phys. Rev. D **90**, 025016 (2014).
 - [28] H. B. Nielsen and M. Ninomiya, Phys. Lett. B **105**, 219 (1981).
 - [29] G. S. Bali, F. Bruckmann, G. Endrodi, Z. Fodor, S. D. Katz, S. Krieg, A. Schafer and K. K. Szabo, JHEP **1202**, 044 (2012).
 - [30] G. V. Dunne, In *Shifman, M. (ed.) et al.: From fields to strings, vol. 1* 445-522.
 - [31] K. Fukushima and P. Morales, in preparation.
 - [32] R. Balbinot and A. Fabbri, Adv. High Energy Phys. **2014**, 713574 (2014).
 - [33] Y. Akamatsu and N. Yamamoto, Phys. Rev. Lett. **111**, 052002 (2013); Phys. Rev. D **90**, no. 12, 125031 (2014).